Journal of Inorganic Biochemistry 196 (2019) 110684

Contents lists available at ScienceDirect

Journal of Inorganic Biochemistry

journal homepage: www.elsevier.com/locate/jinorgbio

# Light-activated ruthenium (II)-bicalutamide prodrugs for prostate cancer

Jian Zhao[a], Nannan Liu[a], Shuchen Sun[a], Shaohua Gou[a,*], Xinyi Wang[a], Zhimei Wang[a], Xiaoyan Li[b], Wenjing Zhang[b,*]

[a] Research Center and School of Chemistry and Chemical Engineering, and Jiangsu Province Hi-Tech Key Laboratory for Biomedical Research, Southeast University, Nanjing 211189, China
[b] The College of Chemistry and Molecular Engineering, Zhengzhou University, Zhengzhou, Henan Province 450001, China

ARTICLE INFO

*Keywords:*
Ruthenium(II) complexes
Photoactivated chemotherapy
Bicalutamide
Anticancer

ABSTRACT

Targeted delivery of clinically approved anticancer drug to tumor sites is an effective way to achieve enhanced drug efficacy as well as reduced side effects and toxicity. Here bicalutamide is caged by the Ru(II) center through the nitrile group, and three photoactive Ru(II) complexes were designed and synthesized. Docking study showed that the ruthenium(II) fragments can effectively block the binding of complexes **1–3** with AR (androgen receptor) owing to the large steric structures, thus bicalutamide in complexes **1–3** could not interact with AR-LBD (ligand binding domain). Once irradiation with blue light (465 nm), complexes **1–3** can release bicalutamide and anticancer Ru(II) fragments, which possesses dual-action of AR binding and DNA interaction simultaneously. In vitro cytotoxicity study on these complexes further confirmed that complexes **1–3** exhibited considerable cytotoxicity upon irradiation with blue light. Significantly, complex **3** could be activated at 660 nm, which greatly increases the scope of complex **3** to treat deeper within tissue. Theoretical calculations showed that the lowest singlet excitation energy of complex **3** is lower than those of complexes **1–2**, which explains the experimental results well. Moreover, the $^{3}$MC (metal centered) states of these complexes are more stable than their $^{3}$MLCT (metal to ligand charge transfer) states, indicating that the photoactive processes of these complexes are likely to result in ligand dissociation.

## 1. Introduction

Prostate cancer is one of the leading causes of cancer death for men worldwide [1]. The development and growth of prostate cancer is found to be initially dependent on androgens, and androgen receptor (AR) is largely involved in the progression of this cancer [2,3]. Therefore, therapeutic strategies by regulating the AR activity can effectively lead to a reduction of prostate cancer [4–9]. Because AR is widely distributed in the human tissues, including the prostate and seminal vesicles, skin, cardiac muscle, adrenal cortex, liver, and so on [10]. Thus, improving the selectivity and activity of the AR antagonist are the key points for the treatment of prostate cancer.

Photoactivated chemotherapy (PACT) is a promising strategy for tumor targeted delivery [11–19], which can be triggered by irradiation to release the active species within the tumor [20–32]. Generally, such agents as prodrugs are kinetically inert and nontoxic in the absence of light, but rapidly give rise to toxic effects upon photoexcitation [33–36]. An ideal candidate for a photoactivatable agent should have the ability to be activated in the “therapeutic window”, 600–850 nm, which enables maximum tissue penetration with minimum damage [29,37–40]. Recently, ruthenium-based PACT agents with high selectivity and low toxicity have been attracting much attention [41–44], as they can be used to deliver a wide variety of bioactive molecules, including enzyme inhibitors, neurotransmitters and so on [45–53]. A majority of clinically approved anticancer drugs are small molecular compounds. Their efficacy has been well studied and established. However, these compounds tend to have wide biodistributions among various tissues after intravenous administration, which may result in widespread systemic toxicity and suboptimal efficacy. Thus, targeted delivery of clinically approved anticancer drugs to tumor sites is an effective way to achieve enhanced drug efficacy and to reduce side effects and toxicity.

In this study, bicalutamide, the most widely used AR antagonist in clinic, is chosen to coordinate to ruthenium(II) fragments through its nitrile group which was reported as an important bioactive “warheads” often engaging in key hydrogen bonding interaction with protein targets [54]. Although the nitrile groups are widely present in medical agents, only a few studies regarding the caging of the bioactive nitriles

* Corresponding authors.
*E-mail addresses:* sgou@seu.edu.cn (S. Gou), zhangwj@zzu.edu.cn (W. Zhang).

https://doi.org/10.1016/j.jinorgbio.2019.03.024
Received 14 January 2019; Received in revised form 25 March 2019; Accepted 28 March 2019
Available online 30 March 2019

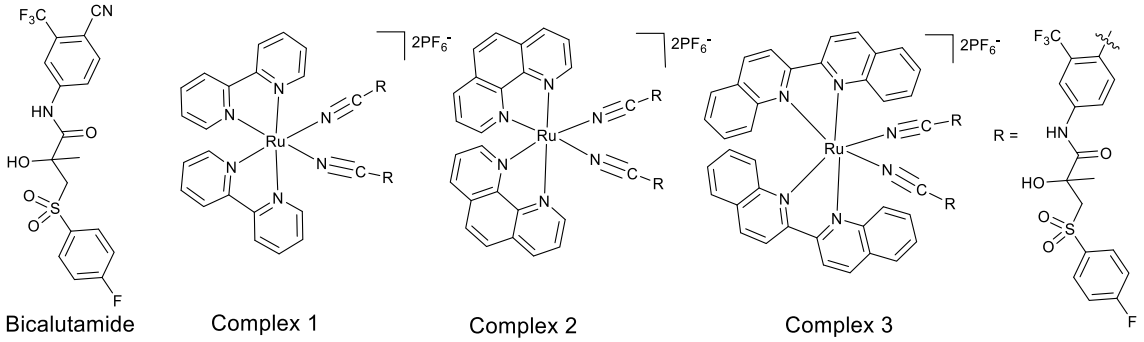


**Fig. 1.** Chemical structures of compounds studied.

through Ru(II) coordination have been reported [55–59]. Herein, three light-activated ruthenium(II) complexes were designed, synthesized and biologically evaluated as potential PACT agents (Fig. 1). Expectedly, the designed compounds can rapidly release bicalutamide upon irradiation at the tumor site and leave the diaquaruthenium(II) moiety to interact with DNA, exhibiting dual-actions against prostate cancer cells.

## 2. Results and discussion

### 2.1. Synthesis and characterization

Complexes **1–3** were prepared by refluxing a mixture of cis-$RuL_2Cl_2$ (L = 2,2′-bipyridine, 1,10-phenanthroline and 2,2′-biquinoline), bicalutamide (4.0 equiv) and silver(I) hexafluorophosphate (2.4 equiv) in ethanol. The target complexes were characterized by $^1$H and $^{13}$C NMR spectroscopy, electrospray ionization mass spectrometry (ESI-MS) and elemental analysis (Figs. S1–9). The ESI-MS diagrams of compounds **1–3** showed the highest isotope at 637.06, 661.06 and 737.14, respectively, corresponding to the dication of $[RuL_2(bicalutamide)_2]^{2+}$. Moreover, $^1$H and $^{13}$C NMR spectra as well as elemental analysis were in good conformity with the proposed molecular structures of complexes **1–3**. The log $P_{OW}$ (the octanol-water partition coefficient) values of the ruthenium(II) complexes were measured using the shake-flask method, which were −0.46, −0.28 and −0.19 for complexes **1–3**, respectively. The stability of complexes **1–3** was evaluated by UV–vis spectral analysis at different times (Fig. S10) [60,61]. No detectable changes of the absorption bands of complexes **1** and **2** have been observed within 15 h, while tiny changes were observed for complex **3**, demonstrating that complexes **1** and **2** were more stable than complex **3**. However, the changes of the absorption bands of complex **3** were very small, indicating that negligible hydrolysis was happened during the test time.

### 2.2. Photolysis study

The photolysis of complexes **1–3** in 98% $H_2O$/2% MeOH was studied under irradiation with blue light (465 nm) by using UV–Vis spectroscopy. UV–Vis spectral changes were obviously observed for these complexes after irradiation (Fig. 2). The metal-to-ligand charge transfer (MLCT) bands at 336 nm and 359 nm for complexes **1** and **2** were gradually replaced by new MLCT bands at 490 nm and 480 nm, respectively. For complexes **1** and **2**, no isosbestic point was observed, indicating that the dissociation reaction was more than one step. As for complex **3**, the initial MLCT was observed at $\lambda_{max}$ = 515 nm, which showed bathochromic shift compared to complexes **1** and **2** [44], demonstrating that the application of biquinoline in complex **3** can decrease the energy gap between the d-orbital of Ru(II) and the lowest unoccupied molecular orbital (LUMO) levels of the ligand. Moreover, complexes **1–3** were studied with irradiation at longer wavelength. Neither **1** nor **2** showed any band changes upon irradiation at 660 nm, whereas complex **3** presented obvious changes under the same condition, confirming that complex **3** could be activated in the PDT (photodynamic therapy) therapeutic window (Fig. S11). The quantum yields of the first step of compounds **1–3** were found to be 0.021, 0.022 and 0.019 in the same test condition (465 nm), respectively. The photolysis of complexes **1** and **3** was further confirmed by $^1$H NMR as well. Complex **1** was stable under 660 nm irradiation, however, it underwent ligand dissociation with irradiation at 465 nm (Fig. S12). Unlike complex **1**, spectral changes were observed for complex **3** after 15 min of irradiation at 660 nm, which is consistent with the UV–Vis results (Fig. S13).

### 2.3. Theoretical calculations

Theoretical calculations were performed to gain further understanding of the photolysis of complexes **1–3**. TDDFT (time-dependent density functional theory) calculations showed that the lowest-energy excited singlet states of complexes **1–3** are $^1$MLLCT (MLLCT = metal-ligand-to-ligand charge transfer) transitions due to the contributions of bicalutamide (Fig. 3) [62], and the corresponding excitation energies of complexes **1–3** are 2.76 eV (449 nm), 2.91 eV (427 nm) and 2.25 eV (551 nm), respectively (Table S1), which is in accord with the experimental results that the absorption tail of complex **3** terminates at relatively longer wavelength as compared with complexes **1–2**. More intense absorption bands indicating the MLLCT transitions are predicted at 320 nm (f = 0.0476), 341 nm (f = 0.0420) and 478 nm (f = 0.0517) for complexes **1–3**, respectively, which also corresponds well with the experimental results.

It is generally accepted that the complexes are first excited by the desired wavelength of light and then undergo intersystem crossing into a $^3$MLCT state, followed by internal conversion to a dissociative $^3$MC state and release of the bicalutamide. Thus, two low-lying triplet states of complexes **1–3** were optimized, corresponding to the $^3$MLCT and $^3$MC states (spin density surfaces). The $^3$MC states of complexes **1–3** corresponds to five-coordinate structures with a bicalutamide dissociated from the Ru center. Notably, the relative energies of $^3$MC states of complexes **1–3** are 0.35 eV, 0.45 eV and 0.28 eV below their $^3$MLCT stats, respectively, indicating that the photoactive process of these complexes is more likely to result in ligand dissociation [63,64].

### 2.4. Docking study

In order to evaluate the likelihood of complexes **1–3** binding to the androgen receptor, a docking study with crystal structure of AR-LBD (ligand binding domain) (PDB: 1z95) was performed [65]. Bicalutamide was firstly docked with the AR-LBD, which was situated inside the binding pocket of AR and showed good overlap with the co-crystallized bicalutamide in the AR crystal structure, proving that the method used is suitable for docking study (Figs. 4a, S16a). However, complexes **1–3** were found to be situated on the surface of the protein (Figs. 4b, S16b, c), which could not enter the ligand binding pocket of AR due to the

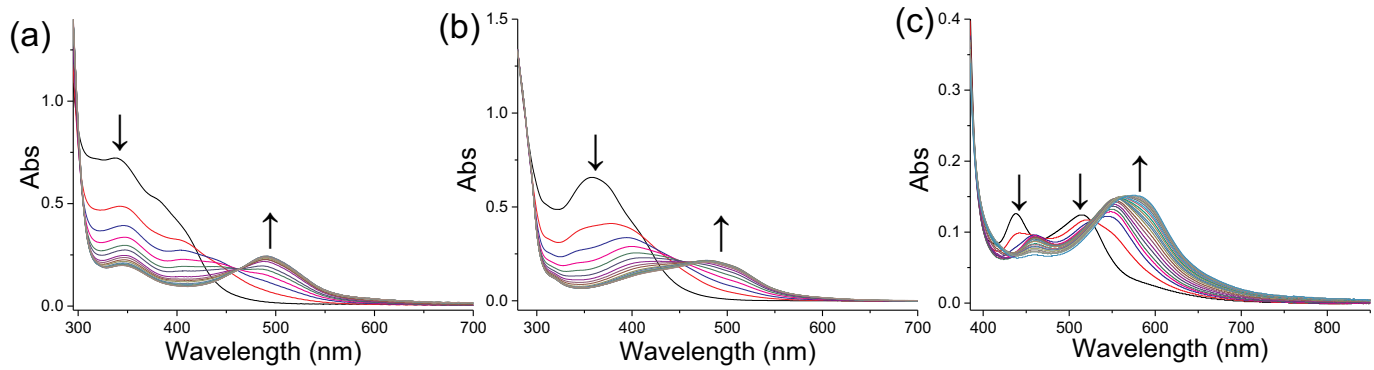


**Fig. 2.** Electronic absorptions of a) complex **1**, b) complex **2**, c) complex **3** (25 μM, 98% $H_2O$/2% MeOH) upon irradiation with blue light ($\lambda_{irr}$ = 465 nm, $t_{irr}$ = 40 min, 10 mW $cm^{-2}$) every 2 min.

large steric structures of the complexes. Moreover, the interaction energies of these complexes with AR were also calculated. As shown in Table S2, the binding energy of the bicalutamide molecule was −9.61 kcal/mol, which was much lower than those of complexes **1–3**, indicating that the ruthenium(II) fragments decreased the binding affinity of bicalutamide with AR. Taken together, this study indicated that the ruthenium(II) fragments of complexes **1–3** can effectively block the binding of bicalutamide with AR owing to their large sizes, implying that complexes **1–3** would be biologically inactive precursors.

### 2.5. AR binding affinity

The AR binding affinity of complexes **1–3** were determined by the fluorescence polarization based binding assay. According to the $IC_{50}$ values (Fig. 4c, Table S3), complexes **1–3** showed negligible AR binding affinity in the dark. In contrast, significant AR binding affinity was observed for complexes **1–3** upon irradiation at 465 nm. Notably, the $IC_{50}$ value of complex **2** was lower than that of bicalutamide, demonstrating that more than one equiv of bicalutamide was released from complex **2**. With irradiation at 660 nm, the binding affinity of complexes **1** and **2** was greatly weakened, while complex **3** maintained the AR binding affinity with an $IC_{50}$ value of 9.2 μM. The result further indicated that complexes **1–3** are biologically inactive precursors, which could be activated upon irradiation with light.

### 2.6. In vitro cytotoxicity

The cytotoxicity and photocytotoxicity of complexes **1–3** were evaluated against AR-negative PC-3 and AR-positive LNCaP cells with bicalutamide as a positive control. According to the $IC_{50}$ values (Table 1), bicalutamide showed moderate cytotoxicity against LNCaP cells with an $IC_{50}$ value of 45.0 μM, which was not affected by irradiation. Complexes **1–3** were found to be less cytotoxic in the dark than bicalutamide against LNCaP cells. However, the antiproliferative activities of complexes **1–3** were greatly improved upon irradiation at 465 nm with PI (phototoxicity index: the toxicity in the dark vs. the light) values of 9.6, 5.3 and 7.7, respectively. The ability of these complexes activated by red light (660 nm) was much attractive, because longer wavelengths of light can penetrate deeper into the tissue with less normal-tissue damage. The cytotoxicity of complexes **1** and **2** greatly decreased upon irradiation at 660 nm compared with irradiation at 465 nm, while that of complex **3** was slightly decreased with a PI value of 5.8. As for PC-3 cells (AR-), bicalutamide showed no apparent activity, exhibiting that the cytotoxicity of bicalutamide is dependent on the expression of AR. In addition, complexes **1–3** had negligible cytotoxicity with or without irradiation (Table S4). Taken together, complexes **1–3** as confirmed could be activated by light, which showed considerable cytotoxicity against AR+ LNCaP cells. Especially, complex **3** could be activated by red light that is known to penetrate tissue deeper.

### 2.7. DNA interaction

The interaction of DNA with complex **3** was monitored by tapping mode atomic force microscopy (AFM) [67]. The image of pBR322 DNA without ruthenium complexes is shown in Fig. 5a. The average height of the DNA was 1.0 nm ($n$ = 15). When complex **3** was added to the solution of DNA, no obvious morphological changes were observed. Once

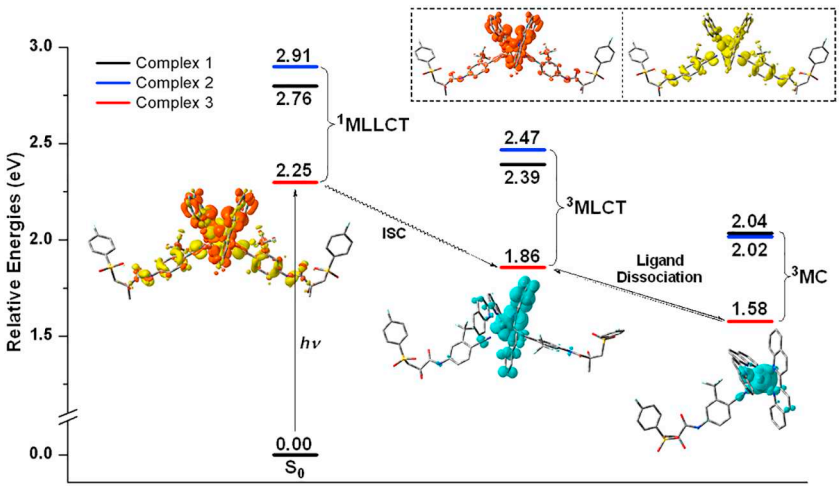


**Fig. 3.** Relative energies of the $^1$MLLCT, $^3$MLCT and $^3$MC states for complexes **1–3**, electron density difference maps (EDDMs) of the lowest-lying singlet transitions (yellow indicates a decrease in charge density, while orange indicates an increase) and spin density of $T_1$ and $^3$MC states for the complex **3**. Both EDDMs and spin density were plotted by the GaussView (version 5.0) program, and those for complexes **1–2** were given in Figs. S14–S15.

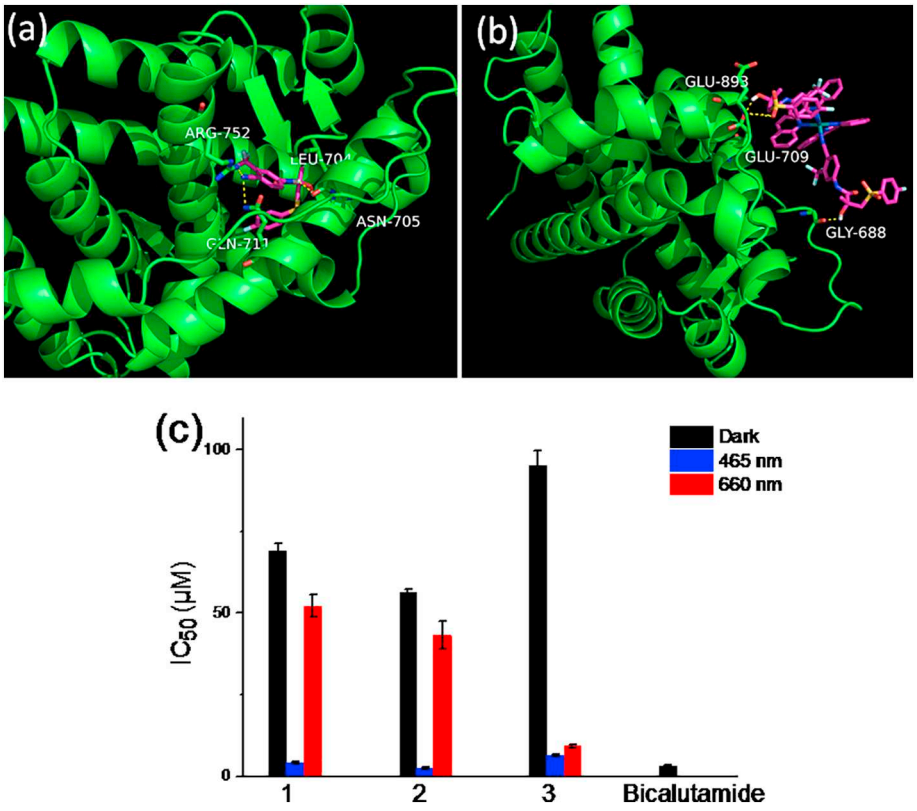


**Fig. 4.** Docking studies of bicalutamide and complex **3** with AR-LBD (PDB: 1z95) using Autodock 4.2 [66]. (a) The docking model of bicalutamide and (b) complex **3** with AR, yellow dash lines represent the H-bond interaction between bicalutamide and complex **3** with AR; (c) AR binding affinity of complexes **1–3** and bicalutamide with or without light irradiation.

**Table 1**
$IC_{50}$ values (μM) and photoselectivity indexes (PI) of complexes **1–3** in LNCaP cells.

| Compound | $IC_{50}$ (μM) | | PI[a] | $IC_{50}$ (μM) | PI[a] |
|---|---|---|---|---|---|
| | Dark | 465 nm | | 660 m | |
| 1 | 85.7 ± 4.8 | 8.9 ± 0.6 | 9.6 | 75.3 ± 3.8 | 1.1 |
| 2 | 71.4 ± 2.5 | 13.6 ± 1.9 | 5.3 | 68.5 ± 4.5 | 1.0 |
| 3 | 91.9 ± 5.7 | 11.9 ± 1.2 | 7.7 | 15.8 ± 1.7 | 5.8 |
| Bicalutamide | 45.0 ± 4.9 | 42.3 ± 3.4 | 1.0 | 47.4 ± 2.1 | 1.0 |

[a] PI = dark $IC_{50}$ value/light $IC_{50}$ value.

irradiation was conducted (465 nm or 660 nm), the formation of reticular structures was observed. This suggested that complex **3** with light irradiation induced crosslinking between DNA molecules by a bridging effect, which are presumably attributed to DNA covalent binding effect.

### 2.8. Gel electrophoresis study

The ability of complex **3** to bind DNA upon light activation was further determined by gel electrophoresis with pBR322 plasmid DNA. As shown in Fig. 6, a decrease in the rate of migration for closed circular DNA (form I) was observed upon 465 nm and 660 nm irradiation, indicating the covalent binding of complex **3** with pBR322 DNA. However, no migration was observed for complex **3** in the dark. Moreover, the plasmid DNA gradually disappeared with increasing concentrations of complex **3**, indicating that complex **3** inhibited the intercalation of EtBr in plasmid DNA at high concentrations. This study indicates that complex 3 can covalently bind to DNA upon irradiation.

### 2.9. Apoptosis study

The potential of these complexes to induce apoptosis in LNCaP cells was performed under light and dark conditions by Hoechst 33342 DNA staining and flow cytometry assay. As shown in Fig. 7, when LNCaP cells were treated with Ru(II) complexes upon irradiation at 465 nm, the typical morphological changes of cell apoptosis such as cell shrinkage and chromatin condensation were observed, while nuclei of the cells retained the regular round contours in the dark, indicating that Ru(II) complexes caused little cell apoptosis without light irradiation. The results were further examined by flow cytometry assay. Under dark conditions, the apoptotic rates of LNCaP cells treated with complexes **1–3** were 16.51%, 15.9%, and 14.42%, respectively, which were slightly increased as compared with that of the untreated cells (6.01%). Once irradiation was conducted (465 nm), the apoptotic rates induced by complexes **1–3** were significantly increased in contrast to the dark group, which ranged from 70.29% to 72.56%. Particularly, when complex **3** was irradiated with 660 nm, the apoptotic rate reached 67.84% which was much higher than the control (9.01%) (Fig. S17).

## 3. Conclusions

Ruthenium(II) polypyridyl complexes are a kind of promising photo-triggered drug delivery system, which offer spatial and temporal control over the release of the bioactive drugs. Herein,

three light-activated Ru(II)-bicalutamide prodrugs were designed and synthesized, which possess both AR binding and DNA interaction actions. Docking studies showed that these complexes could not enter the ligand binding pocket of AR due to the large steric structures of the Ru(II) fragments, implying that they would be biologically inactive precursors. However, when irradiated with blue light (465 nm), these complexes could release both bicalutamide and anticancer Ru(II) fragments to inhibit the growth of cancer cells via different modes of action. In vitro cytotoxicity study confirmed that complexes **1–3** could be activated upon photoexcitation with blue light, exhibiting considerable cytotoxicity against the LNCaP (AR+) cells. Significantly, the anticancer activity of complex **3** was also retained when irradiated by red light (660 nm), hinting that complex **3** could be activated in the PDT therapeutic window. Theoretical calculations showed that the singlet

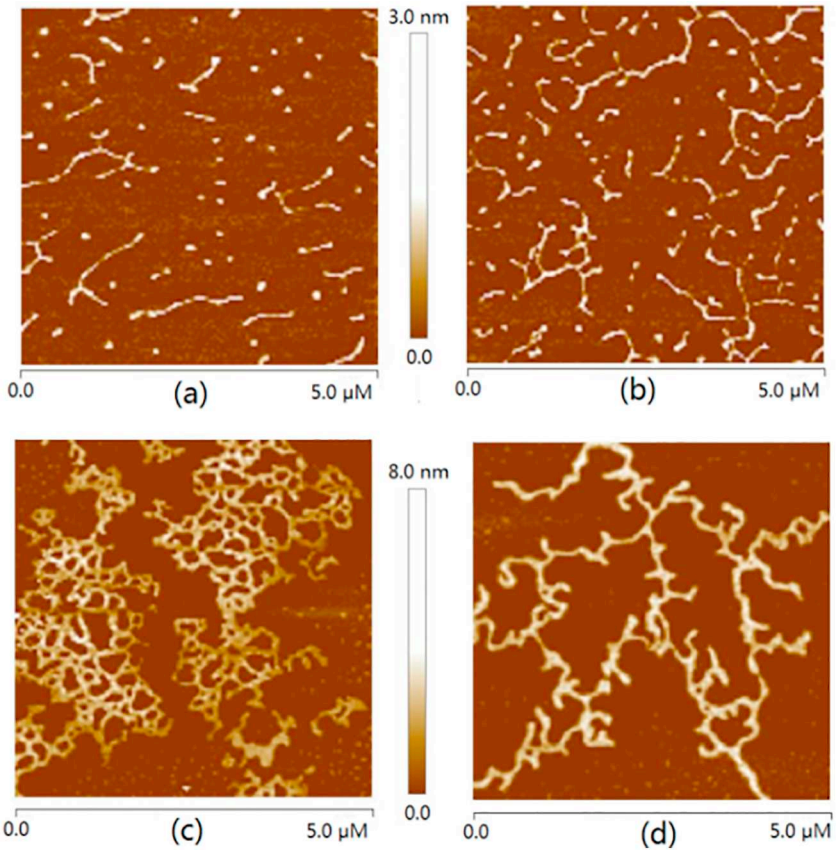


**Fig. 5.** AFM images of pBR322 plasmid DNA in HEPES (*N*-2-hydroxyethylpiperazine-*N*′-2-ethanesulfonic acid) buffer adsorbed on peeled mica: (a) images of pBR322 plasmid alone; (b) incubated with complex **3** in dark; (c) incubated with complex **3** upon irradiation at 465 nm; and (d) incubated with complex **3** upon irradiation at 660 nm.

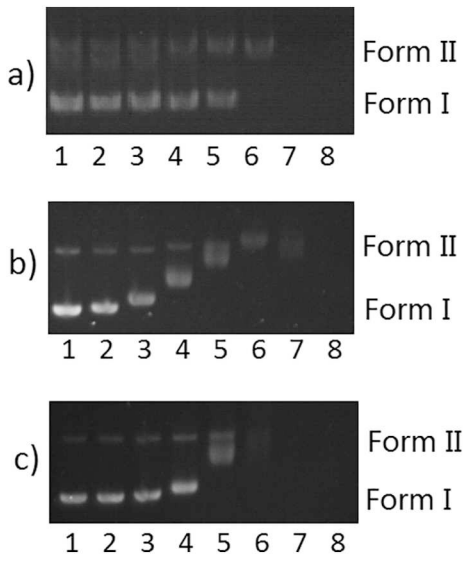


**Fig. 6.** Gel electrophoretic mobility pattern of pBR322 plasmid DNA incubated with various concentrations of complex **3**. Lane 1–8 (0, 10, 20, 40, 80, 160, 320, 640 μM) + DNA. a) dark; b) irradiation at 465 nm for; c) irradiation at 660 nm.

excited energy of complex **3** is lower than those of complexes **1–2**, which can explain the experimental results well. Moreover, the $^{3}$MC states of these complexes are more stable than their $^{3}$MLCT state, indicating that the photoactive processes of these complexes are more likely to cause ligand dissociation. In all, our study indicated that caging of bicalutamide through its nitrile group is an efficient way to increasing its selectivity. Therefore, photocaging of clinically approved anticancer drugs using ruthenium(II) polypyridyl complexes is an effective way to discover new clinical agents.

## 4. Materials and methods

### 4.1. Materials and instrument

All chemicals and solvents were of analytical reagent grade and used without further purification. Bicalutamide was obtained from Aladdin as a racemic mixture of the R and S enantiomers and used as received. Cis-$RuL_2Cl_2$ (L = 2,2′-bipyridine, 1,10-phenanthroline and 2,2′-biquinoline) were prepared according to previous reports [37,68]. $^{1}$H and $^{13}$C NMR spectra were measured on Bruker Avance III-HD 600 MHz spectrometer. UV–Vis spectra and kinetic traces were recorded on a Shimadzu UV2600 instrument. Mass spectra were measured by an Agilent 6224 ESI/TOF MS (electrospray-ionization time-of-flight mass spectrometry) instrument. Elemental analysis of C, H, and N used a Vario MICRO CHNOS elemental analyzer (Elementar). Cancer cells were obtained from Jiangsu KeyGEN BioTECH company(China). Cell apoptosis experiments were measured by flow cytometry (FAC Scan, Becton Dickenson) and analyzed by Cell Quest software.

### 4.2. Preparation of compounds

General procedure for synthesis of complexes **1–3**. A methanol solution (50 mL) of $RuL_2Cl_2$ (0.20 mM), $AgPF_6$ (0.12 g, 0.48 mM) and bicalutamide (0.34 g, 0.8 mM) was heated at reflux for 12 h in the absence of light. Then the solution was filtered to remove AgCl and the reaction mixture was concentrated to 5 mL. The crude product was collected and recrystallized from methanol. Complexes **1–3** were isolated as racemic mixtures (see supporting Fig. S18).

Complex **1**. Yield: 0.16 g (50.6%). Dark-red powder. Anal. Calcd (%) for $C_{56}H_{44}F_{20}N_8O_8P_2RuS_2$: C 43.00, H 2.84, N 7.16. Found: C 43.09, H 2.88, N 7.08; ESI-MS: $m/z$ $[M/2 - PF_6]^+$ = 637.06; $^{1}$H NMR (600 MHz, DMSO-$d_6$) $\delta$ 1.38 (s, 6H), 3.72 (s, 1H), 3.74 (s, 1H), 3.90 (s, 1H), 3.93(s, 1H), 6.46 (m, 2H), 7.36–7.39 (t, 4H, $J$ = 8.8 Hz), 7.48–7.51 (t, 2H,

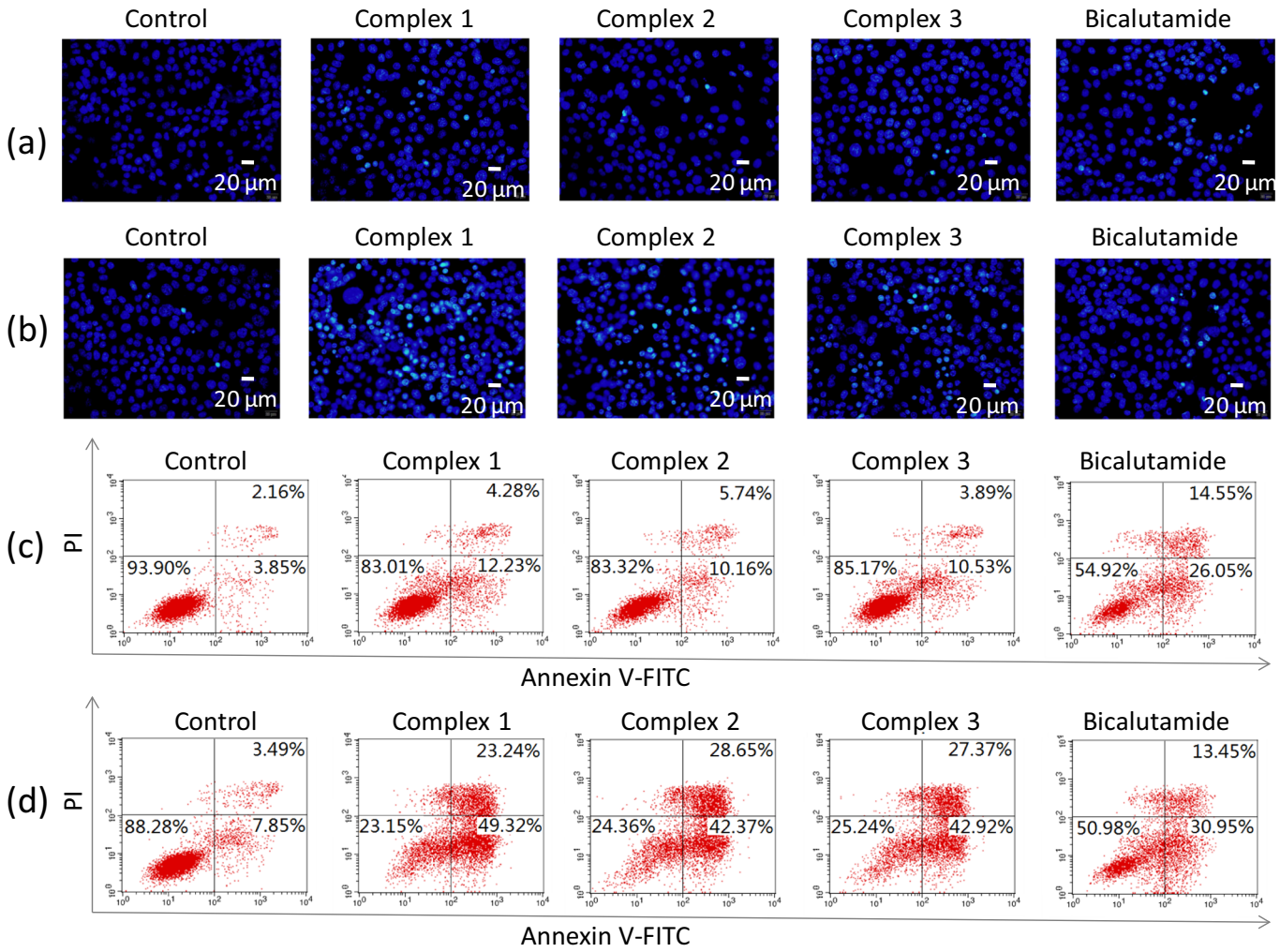


**Fig. 7.** Cell apoptosis induction on LNCaP cells after treatment with complexes **1–3** and cisplatin at 30 μM: morphological changes with Hoechst 33342 staining in the absence (a) and presence blue light (b); Flow cytometry analysis for apoptosis of LNCaP cells in the absence (c) and presence blue light (d).

$J$ = 6.7 Hz), 7.78–7.79 (d, 2H, $J$ = 5.4 Hz), 7.90–7.92 (m, 4H), 8.00–8.02 (t, 2H, $J$ = 6.5 Hz), 8.16–8.19 (t, 2H, $J$ = 7.9 Hz), 8.26 (m, 4H), 8.36 (m, 2H), 8.45–8.48 (m, 2H), 8.80–8.82 (d, 2H, $J$ = 8.2 Hz), 8.93–8.94 (d, 2H, $J$ = 8.3 Hz), 9.48–9.49 (d, 2H, $J$ = 5.4 Hz), 10.44 (m, 2H) ppm; $^{13}$C NMR (150 MHz, DMSO-$d_6$) $\delta$ 16.97, 26.47, 56.94, 63.60, 73.22, 100.81, 115.66, 115.81, 117.46, 121.29, 122.41, 122.48, 123.10, 123.74, 124.09, 127.10, 128.05, 131.36, 131.43, 133.52, 133.73, 136.87, 136.89, 137.12, 138.64, 138.97, 143.69, 151.71, 153.43, 157.00, 157.73, 164.90, 166.58, 173.98 ppm.

Complex **2**. Yield: 0.17 g (52.3%). Dark-red powder. Anal. Calcd (%) for $C_{60}H_{44}F_{20}N_8O_8P_2RuS_2$: C 44.70, H 2.75, N 6.95. Found: C 44.79, H 2.74, N 6.86; ESI-MS: $m/z$ $[M/2 - PF_6]^+$ = 661.06; $^1$H NMR (600 MHz, $CD_3OD$) $\delta$ 1.32 (s, 6H), 3.46 (s, 1H), 3.49 (s, 1H), 3.86 (s, 1H), 3.89 (s, 1H), 5.38 (m, 1H), 7.07–7.10 (m, 4H), 7.49–7.52 (d-d, 2H, $J$ = 5.3, 2.8 Hz), 7.79–7.81 (m, 4H), 7.89–7.94 (m, 4H), 7.98–7.99 (d, 2H, $J$ = 8.7 Hz), 8.03–8.04 (m, 2H), 8.15–8.16 (d, 2H, $J$ = 8.9 Hz), 8.23–8.26 (m, 2H), 8.28–8.29 (d, 2H, $J$ = 8.9 Hz), 8.50–8.52 (d, 2H, $J$ = 8.2 Hz), 8.88–8.89 (m, 2H), 9.83–9.84 (d, 2H, $J$ = 5.1 Hz) ppm; $^{13}$C NMR (150 MHz, $CD_3OD$) $\delta$ 26.45, 63.57, 73.19, 100.81, 115.63, 115.79, 117.32, 121.04, 122.40, 122.62, 125.46, 126.59, 127.67, 127.89, 130.77, 131.11, 131.34, 131.40, 133.41, 133.62, 136.87, 137.04, 137.51, 137.95, 143.59, 147.71, 148.18, 152.77, 154.52, 164.87, 166.56, 173.93 ppm.

Complex **3**. Yield: 0.22 g (61.3%). Dark-red powder. Anal. Calcd (%) for $C_{72}H_{52}F_{20}N_8O_8P_2RuS_2$: C 49.01, H 2.97, N 6.35. Found: C 49.12, H 2.96, N 6.37; ESI-MS: m/z $[M/2 - PF_6]^+$ = 737.14; $^1$H NMR (600 MHz, $CD_3OD$) $\delta$ 1.30 (s, 6H), 3.45 (s, 1H), 3.47 (s, 1H), 3.85 (s, 1H), 3.89 (s, 1H), 6.77–6.84 (m, 4H), 7.04–7.08 (m, 4H), 7.44–7.46 (t, 2H, $J$ = 7.4 Hz), 7.77–7.80 (m, 4H), 7.86–7.87 (d, 2H, $J$ = 7.9 Hz), 7.91–8.00 (m, 10H), 8.09–8.10 (m, 2H), 8.28–8.30 (d, 2H, $J$ = 8.0 Hz), 8.34–8.36 (m, 4H), 8.69–8.70 (d, 2H, $J$ = 8.6 Hz), 9.62 (m, 2H) ppm; $^{13}$C NMR (150 MHz, $CD_3OD$) $\delta$ 26.43, 53.41, 63.51, 73.14, 100.64, 115.61, 115.76, 117.37, 118.84, 120.05, 121.00, 122.45, 122.81, 123.42, 127.51, 128.87, 129.09, 129.70, 130.00, 131.33, 131.40, 133.05, 133.27, 133.83, 136.74, 137.06, 140.05, 140.71, 143.88, 149.17, 150.43, 160.36, 160.59, 164.85, 166.53, 173.86 ppm.

### 4.3. Log $P_{OW}$ determination

The log $P_{OW}$ determination of complexes **1–3** was performed using the shake-flask method. An excess of complexes **1–3** was dissolved in double-distilled water presaturated with n-octanol for 24 h at 37 °C. The solution was filtered to remove undissolved ruthenium complexes. Subsequently, the solution was added to an equal volume of n-octanol (presaturated with water). The heterogeneous mixture was shaken for 2 h before centrifuging for 15 min to achieve phase separation. The initial and final concentrations of compounds in an aqueous phase were determined by the UV–vis spectrum method, and the water-octanol partition coefficients (log $P_{OW}$) were calculated.

### 4.4. Photolysis study

Photolysis of complexes **1–3** was recorded on a Shimadzu UV2600 instrument equipped with a thermostatically controlled cell holder. Stock solutions of **1–3** were prepared in methanol and diluted with water to give a final water/methanol composition of 98:2. The cuvette was irradiated with a directional LED light at 465 ± 10 nm (10 mW $cm^{-2}$) or 660 ± 10 nm (50 mW $cm^{-2}$), and the output power density of the LED was controlled by an LED controller. UV–Vis absorbance spectra were recorded at regular intervals (2 min for 465 nm irradiation, 5 min for 660 nm). Ferrioxalate actinometry was used as a reference to determine the photon flux of our LED light source. The quantum yields of the first step of complexes **1–3** were calculated according to the method described before [57]

### 4.5. DFT calculation

All calculations were performed using the Gaussian 09 suit of program [69]. The ground state ($S_0$), the lowest-lying triplet state ($T_1$), and the dissociated structures of complexes **1–3** were optimized by using the B3LYP density functional [70] with the LanL2DZ basis set and effective core functional [71] used for the Ru atom while the 6-31G(d) basis set [72,73] for the other atoms. All structures were confirmed to be minima by harmonic vibrational frequency calculations. The time-dependent density functional theory (TD-DFT) [74–76] calculations were performed at the same level to predict the singlet electronic transitions and the UV–visible spectra. The $^3$MLCT, and $^3$MC electronic configurations were characterized by examining the spin densities, and the $^1$MLLCT state were identified by analyzing the molecular orbital populations. The electron density difference maps (EDDMs) of the lowest-lying singlet transitions of the three complexes were plotted by the GaussView(version 5.0).

### 4.6. Docking study

Docking studies were carried out using Autodock Dock 4.2. The crystal structure of AR-LBD (ligand binding domain) was obtained from the Protein Data Bank (PDB ID: 1z95). Bicalutamide in 1z95 were removed prior to the docking by software PyMOL. The docking simulation was performed with the Lamarckian genetic algorithm for as much as 150 docking runs. Each run of the docking operation was terminated after a maximum of 2,500,000 energy evaluations. During docking studies, the protein structure was kept rigid. Rotation in the complexes **1–3** was permitted about all single bonds.

### 4.7. AR ligand binding affinity

The fluorescence polarization technique was applied to study the binding of complexes **1–3** and bicalutamide to the androgen receptor using the PolarScreen™ AR Competitor Assay, Green (lifetechnologies, A15880) according to the manufacturer's instructions. Complexes **1–3** with desired concentrations were irradiated with a directional LED light at 465 nm (30 min) or 660 nm (1 h), and then were titrated against a preformed complex of Fluormone™ AL Green and the AR-LBD (GST). The assay mixture was incubated at room temperature for 4 h, after which the fluorescence polarization values were measured in a SpectraMax® Paradigm® Multi-Mode Detection Platform using an excitation wavelength of 485 nm and an emission wavelength of 535 nm. Data analysis for the ligand binding assays was performed using GraphPad Prism software.

### 4.8. Atomic force microscopy (AFM)

The pBR322 plasmid DNA (200 ng/μL) was diluted to 5 ng/μL with hepes (*N*-2-hydroxyethylpiperazine-*N*′-2-ethanesulfonic acid) buffer (40 mM hepes, 5 mM $MgCl_2$, pH 7.4). Complex **3** was dissolved in DMF first and then diluted to 0.5 mM with hepes buffer (the final concentration of DMF was less than 0.4%). The solutions of complex **3** (20 μL) and pBR322 (20 μL) were mixture together, and irradiated with blue light (465 nm, 30 min) or red light (660 nm, 1 h). After 24 h incubation, the mixture was dropped onto freshly cleaved mica. Then the samples were rinsed for 10 s with deionized water and dried with nitrogen gas. The images were obtained in air at room temperature on areas of 5 × 5 $\mu m^2$.

### 4.9. Gel electrophoresis study

DNA binding properties of complex **3** was also investigated by agarose gel electrophoresis. Desired concentrations of the complex **3** were prepared by dilution of the compound with Tris-$H_3PO_4$ (100 mm) buffer. pBR322 DNA (5 μL) was added to each tube. The mixtures of complex **3** and pBR322 plasmid DNA were mixture together, and irradiated with blue light (465 nm, 30 min) or red light (660 nm, 1 h). After 24 h incubation, the agarose gel (made up to 1% w/v) was prepared with TA buffer (50 mm Tris-acetate, pH 7.4). The mixtures with loading buffer (1 mL) were submitted to electrophoresis in agarose gel in TA buffer at 100 V for 90 min. Agarose gels were then dyed with ethidium bromide (0.5 mg/L) for 20 min. Bands were imaged by using a Molecular Imager (Bio-Rad, USA) under UV light.

### 4.10. MTT assay

Cytotoxicity of complexes **1–3** and bicalutamide against LNCaP and PC-3 cells was determined by means of the MTT (3-(4,5-dimethylthiazol-2-yl)-2,5-diphenyl tetrazolium bromide) assay. Cells were cultured in RPMI-1640 medium with 10% fetal bovine serum (FBS). All media were also supplemented with 100 mg/mL of penicillin and 100 mg/mL of streptomycin. Cells (105 per well) with better vitality were seeded in 96-well plates. The compounds were dissolved by DMF and diluted with medium to various concentrations (the final concentration of DMF was less than 0.4%). After being incubated in the dark for 4 h, cells were irradiated with blue light (465 nm) for 30 min or red light (660 nm) for 1 h, and then the cells were incubated in the dark for a further 48 h. After that, cells were stained with 3-(4,5-dimethyl-2-thiazolyl)-2,5-diphenyl-2Htetrazolium bromide (MTT) (5 mg/mL) for another 5 h, and then the medium was thrown away and replaced by 150 mL DMSO. The inhibition of cell growth induced by the tested complexes was detected by measuring the absorbance of each well at 570/630 nm using enzyme labeling instrument. The $IC_{50}$ values were calculated by SPSS software after three parallel experiments.

### 4.11. Apoptosis assessment by Hoechst 33342 staining

LNCaP cells were seeded in 24-well plates at 1 × $10^5$ cells/well and incubated overnight. Cells were incubated with 30 μM of the tested compounds, and then irradiated with blue light (465 nm, 30 min) or red light (660 nm, 1 h). The cells were incubated in the dark for a further 24 h. After that, the cells were rinsed twice in PBS (phosphate-buffered saline) and stained with Hoechst 33342 fluorescent dye for 10 min in the dark at 37 °C. Cell apoptosis was examined under the fluorescence microscope with excitation wavelength of 330–380 nm.

### 4.12. Apoptosis analysis by flow cytometry

LNCaP cells were grown in a 6-well plate and cultured overnight. The tested complexes were added with the final concentration of 30 μM. After incubation for 24 h, cells were irradiated with blue light (465 nm, 30 min) or red light (660 nm, 1 h). After that, the cells were incubated in the dark for a further 24 h, and collected by centrifugation (5 min, 25 °C, 2000 rpm). Then, the cells were washed twice with cold water, resuspended in binding buffer (10 mM hepes, 140 mM NaCl, 2.5 mM $CaCl_2$, pH 7.4). The cells were stained with 5 μL of Annexin V-

FITC (fluorescein isothiocyanate) and then with 5 μL of propidium iodide (20 μg/mL) for 15 min in the dark at room temperature. The fluorescence of cells was detected by an annexin V-FITC apoptosis detection kit (Roche) according to the manufacturer's protocol, and cells were quantified by system software (Cell Quest; BD Biosciences).

## Acknowledgments

We are grateful to the National Natural Science Foundation of China (Grant No. 21601034 and 21503191) and Jiangsu Province Natural Science Foundation (Grant No. BK20160664) for financial aids to this work. We also thank the Fundamental Research Funds for the Central Universities (Project 2242016K30020 and 2242017K41025) and Priority Academic Program Development of Jiangsu Higher Education Institutions for the construction of fundamental facilities are also appreciated.

## Conflicts of interest

There are no conflicts to declare.

## Appendix A. Supplementary data

Supplementary data to this article can be found online at https://doi.org/10.1016/j.jinorgbio.2019.03.024.

## References

[1] L.A. Torre, F. Bray, R.L. Siegel, J. Ferlay, J. Lortet-tieulent, A. Jemal, Ca-Cancer J. Clin. 65 (2015) 87–108.
[2] C.D. Chen, D.S. Welsbie, C. Tran, S.H. Baek, R. Chen, R. Vessella, M.G. Rosenfeld, C.L. Sawyers, Nat. Med. 10 (2004) 33–39.
[3] T. Visakorpi, E. Hyytinen, P. Koivisto, M. Tanner, R. Keinanen, C. Palmberg, A. Palotie, T. Tammela, J. Isola, O.P. Kallioniemi, Nat. Genet. 9 (1995) 401–406.
[4] C. Ferroni, A. Pepe, Y.S. Kim, S. Lee, A. Guerrini, M.D. Parenti, A. Tesei, A. Zamagni, M. Cortesi, N. Zaffaroni, J. Med. Chem. 60 (2017) 3082–3093.
[5] S.P. Balk, Urology 60 (2002) 132–138.
[6] S. Zhao, Y. Shen, A. van Oeveren, K.B. Marschke, L. Zhi, Bioorg. Med. Chem. Lett. 18 (2008) 3431–3435.
[7] G.J. Kolvenbag, G.R. Blackledge, K. Gotting-Smith, Prostate 34 (1998) 61–72.
[8] H.I. Scher, T.M. Beer, C.S. Higano, A. Anand, M.E. Taplin, E. Efstathiou, D. Rathkopf, J. Shelkey, E.Y. Yu, J. Alumkal, Lancet 375 (2010) 1437–1446.
[9] V. Rapozzi, D. Ragno, A. Guerrini, C. Ferroni, E.D. Pietra, D. Cesselli, G. Castoria, M. Di Donato, E. Saracino, V. Benfenati, Bioconjugate. Chem. 26 (2015) 1662–1671.
[10] A. Negro-Vilar, J. Clin. Endocrinol. Metab. 84 (1999) 3459–3462.
[11] N.J. Farrer, L. Salassa, P.J. Sadler, Dalton Trans. 0 (2009) 10690–10701.
[12] A. Li, C. Turro, J.J. Kodanko, Acc. Chem. Res. 51 (2018) 1415–1421.
[13] S. Bonnet, Dalton Trans. 47 (2018) 10330–10343.
[14] M. Imran, W. Ayub, I.S. Butler, Coord. Chem. Rev. 376 (2018) 405–429.
[15] J.D. Knoll, B.A. Albaniand, C. Turro, Acc. Chem. Res. 48 (2015) 2280–2287.
[16] W. Szymanski, Curr. Med. Chem. 24 (2017) 4905–4950.
[17] H. Shi, I. Romero-Canelón, M. Hreusova, O. Novakova, V. Venkatesh, A. Habtemariam, G.J. Clarkson, J. Song, V. Brabec, P.J. Sadler, Inorg. Chem. 57 (2018) 14409–14420.
[18] A. Bjelosevic, B.J. Pages, L.K. Spare, K.M. Deo, D.L. Ang, J.R. Aldrich-Wright, Curr. Med. Chem. 25 (2018) (478-49).
[19] A. Bahreman, J. Cuellogaribo, S. Bonnet, Dalton Trans. 43 (2014) 4494–4505.
[20] S.C. Marker, S.N. MacMillan, W.R. Zipfel, Z. Li, P.C. Ford, J.J. Wilson, Inorg. Chem. 57 (2018) 1311–1331.
[21] K. Arora, M. Herroon, M.H. Al-Afyouni, N.P.T.N. Toupin, L.M. Rohrabaugh Jr., M. Loftus, I. Podgorski, C. Turro, J.J. Kodanko, J. Am. Chem. Soc. 140 (2018) 14367–14380.
[22] L.N. Lameijer, C. van de Griend, S.L. Hopkins, A.G. Volbeda, S.H.C. Askes, M.A. Siegler, S. Bonnet, J. Am. Chem. Soc. 141 (2018) 352–362.
[23] J.J. Woods, J. Cao, A.R. Lippert, J.J. Wilson, J. Am. Chem. Soc. 140 (2018) 12383–12387.
[24] L.N. Lameijer, T.G. Brevé, V.H. van Rixel, S.H.C. Askes, M.A. Siegler, S. Bonnet, Chem. Eur. J. 24 (2018) 2709–2717.
[25] R.N. Pickens, B.J. Neyhouse, D.T. Reed, S.T. Ashton, J.K. White, Inorg. Chem. 57 (2018) 11616–11625.
[26] N. Karaoun, A.K. Renfrew, Chem. Commun. 51 (2015) 14038–14041.
[27] J.C. Griepenburg, T.L. Rapp, P.J. Carroll, J. Eberwine, I.J. Dmochowski, Chem. Sci. 6 (2015) 2342–2346.
[28] N.A. Smith, P. Zhang, S.E. Greenough, M.D. Horbury, G.J. Clarkson, D. McFeely, A. Habtemariam, L. Salassa, V.G. Stavros, C.G. Dowson, P.J. Sadler, Chem. Sci. 8 (2017) 395–404.
[29] M.A. Sgambellone, A. David, R.N. Garner, K.R. Dunbar, C. Turro, J. Am. Chem. Soc. 135 (2013) 11274–11282.
[30] L.N. Lameijer, D. Ernst, S.L. Hopkins, M.S. Meijer, S.H. Askes, S.E. Le Devedec, S. Bonnet, Angew. Chem. Int. Ed. 56 (2017) 11549–11553.
[31] W. Sun, S. Li, B. Haupler, J. Liu, S. Jin, W. Steffen, U.S. Schubert, H. Butt, X. Liang, S. Wu, Adv. Mater. 29 (2017) 1603702.
[32] A. Leonidova, V. Pierroz, R. Rubbiani, Y. Lan, A.G. Schmitz, A. Kaech, R.K.O. Sigel, S. Ferrari, G. Gasser, Chem. Sci. 5 (2014) 4044–4056.
[33] J. Liu, C. Zhang, T.W. Rees, L. Ke, L. Ji, H. Chao, Coord. Chem. Rev. 363 (2018) 17–28.
[34] D. Havrylyuk, M. Deshpande, S. Parkin, E.C. Glazer, Chem. Commun. 54 (2018) 12487–12490.
[35] A. Soupart, F. Alary, J.L. Heully, P.I.P. Elliott, I.M. Dixon, Inorg. Chem. 57 (2018) 3192–3196.
[36] E. Wachter, B.S. Howerton, E.C. Hall, S. Parkin, E.C. Glazer, Chem. Commun. 50 (2014) 311–313.
[37] E. Wachter, D.K. Heidary, B.S. Howerton, S. Parkin, E.C. Glazer, Chem. Commun. 48 (2012) 9649–9651.
[38] L.M. Loftus, K.F. Al-Afyouni, C. Turro, Chem. Eur. J. 24 (2018) 11550–11553.
[39] M.H. Al-Afyouni, T.N. Rohrabaugh, K.F. Al-Afyouni, C. Turro, Chem. Sci. 9 (2018) 6711–6720.
[40] W. Sun, R. Thiramanas, L.D. Slep, X. Zeng, V. Mailander, S. Wu, Chem. Eur. J. 23 (2017) 10832–10837.
[41] J. Wei, A.K. Renfrew, J. Inorg. Biochem. 179 (2018) 146–153.
[42] A. Li, R. Yadav, J.K. White, M.K. Herroon, B.P. Callahan, I. Podgorski, C. Turro, E.E. Scott, J.J. Kodanko, Chem. Commun. 53 (2017) 3673–3676.
[43] A. Zamora, C.A. Denning, D.K. Heidary, E. Wachter, L.A. Nease, J. Ruiza, E.C. Glazer, Dalton Trans. 46 (2017) 2165–2173.
[44] J.A. Cuello-Garibo, C.C. James, M.A. Siegler, S.L. Hopkins, S. Bonnet, Chem. Eur. J. 25 (2019) 1260–1268.
[45] A.K. Renfrew, Metallomics 6 (2014) 1324–1335.
[46] L. Zayat, C. Calero, P. Albores, L.M. Baraldo, R. Etchenique, J. Am. Chem. Soc. 125 (2003) 882–883.
[47] F. Qu, S. Park, K. Martinez, J.L. Gray, F.S. Thowfeik, J.A. Lundeen, A.E. Kuhn, D.J. Charboneau, D.L. Gerlach, M.M. Lockart, Inorg. Chem. 56 (2017) 7519–7532.
[48] B. Siewert, M. Langerman, Y. Hontani, J. Kennis, V. van Rixel, B. Limburg, M. Siegler, V.T. Saez, R. Kieltyka, S. Bonnet, Chem. Commun. 53 (2017) 11126–11129.
[49] J. Mosquera, M.I. Sanchez, J.L. Mascarenas, M.E. Vazquez, Chem. Commun. 51 (2015) 5501–5504.
[50] J.-A. Cuello-Garibo, M.S. Meijer, S. Bonnet, Chem. Commun. 53 (2017) 6768–6771.
[51] A.N. Hidayatullah, E. Wachter, D.K. Heidary, S. Parkin, E.C. Glazer, Inorg. Chem. 53 (2014) 10030–10032.
[52] J.D. Knoll, B.A. Albani, C. Turro, Chem. Commun. 51 (2015) 8777–8780.
[53] T.N. Rohrabaugh, A.M. Rohrabaugh, J.J. Kodanko, J.K. White, C. Turro, Chem. Commun. 54 (2018) 5193–5196.
[54] F.F. Fleming, L. Yao, P.C. Ravikumar, L.A. Funk, B.C. Shook, J. Med. Chem. 53 (2010) 7902–7917.
[55] R.N. Garner, J.C. Gallucci, K.R. Dunbar, C. Turro, Inorg. Chem. 50 (2011) 9213–9215.
[56] T. Respondek, R.N. Garner, M.K. Herroon, I. Podgorski, C. Turro, J.J. Kodanko, J. Am. Chem. Soc. 133 (2011) 17164–17167.
[57] T. Respondek, R. Sharma, M.K. Herroon, R.N. Garner, J.D. Knoll, E. Cueny, C. Turro, I. Podgorski, J.J. Kodanko, Chem. Med. Chem. 9 (2014) 1306–1315.
[58] A. Li, C. Turro, J.J. Kodanko, Chem. Commun. 54 (2018) 1280–1290.
[59] B.A. Albani, C.B. Durr, C. Turro, J. Phys. Chem. A 117 (2013) 13885–13892.
[60] J. Zhao, S. Gou, Y. Sun, L. Fang, Z. Wang, Inorg. Chem. 51 (2012) 10317–10324.
[61] J. Zhao, W. Li, S. Gou, S. Li, S. Lin, Q. Wei, G. Xu, Inorg. Chem. 57 (2018) 8396–8403.
[62] L. Salassa, C. Garino, G. Salassa, R. Gobetto, C. Nervi, J. Am. Chem. Soc. 130 (2008) 9590–9597.
[63] Y.J. Tu, S. Mazumder, J.F. Endicott, C. Turro, J.J. Kodanko, H.B. Schlegel, Inorg. Chem. 54 (2015) 8003–8011.
[64] K. Nisbett, Y.J. Tu, C. Turro, J.J. Kodanko, H.B. Schlegel, Inorg. Chem. 57 (2017) 231–240.
[65] C.E. Bohl, W. Gao, D.D. Miller, C.E. Bell, J.T. Dalton, Proc. Natl. Acad. Sci. U. S. A. 102 (2005) 6201–6206.
[66] G.M. Morris, R. Huey, W. Lindstrom, M.F. Sanner, R.K. Belew, D.S. Goodsell, A.J. Olson, J. Comput. Chem. 30 (2009) 2785–2791.
[67] J. Zhao, S. Li, X. Wang, G. Xu, S. Gou, Inorg. Chem. 58 (2019) 2208–2217.
[68] B.P. Sullivan, D.J. Salmon, T.J. Meyer, Inorg. Chem. 17 (1978) 3334–3341.
[69] M.J. Frisch, G.W. Trucks, H.B. Schlegel, G.E. Scuseria, M.A. Robb, J.R. Cheeseman, G. Scalmani, V. Barone, B. Mennucci, G.A. Petersson, H. Nakatsuji, M. Caricato, X. Li, H.P. Hratchian, A.F. Izmaylov, J. Bloino, G. Zheng, J.L. Sonnenberg, M. Hada, M. Ehara, K. Toyota, R. Fukuda, J. Hasegawa, M. Ishida, T. Nakajima, Y. Honda, O. Kitao, H. Nakai, T. Vreven, J.A. Montgomery, J.E. P. Jr., F. Ogliaro, M. Bearpark, J.J. Heyd, E. Brothers, K.N. Kudin, V.N. Staroverov, T. Keith, R. Kobayashi, J. Normand, K. Raghavachari, A. Rendell, J.C. Burant, S.S. Iyengar, J. Tomasi,

M. Cossi, N. Rega, J.M. Millam, M. Klene, J.E. Knox, J.B. Cross, V. Bakken, C. Adamo, J. Jaramillo, R. Gomperts, R.E. Stratmann, O. Yazyev, A.J. Austin, R. Cammi, C. Pomelli, J.W. Ochterski, R.L. Martin, K. Morokuma, V.G. Zakrzewski, G.A. Voth, P. Salvador, J.J. Dannenberg, S. Dapprich, A.D. Daniels, O. Farkas, J.B. Foresman, J.V. Ortiz, J. Cioslowski, D.J. Fox, Gaussian 09, Revision C. 01, Gaussian, Inc., Wallingford CT, 2010.
[70] P.J. Stephens, F.J. Devlin, C.F. Chabalowski, M.J. Frisch, J. Phys. Chem. 98 (1994) 11623–11627.
[71] W.R. Wadt, P.J. Hay, J. Chem. Phys. 82 (1985) 284–298.
[72] M.M. Francl, W.J. Pietro, W.J. Hehre, J.S. Binkley, M.S. Gordon, D.J. Defrees, J.A. Pople, J. Chem. Phys. 77 (1982) 3654–3665.
[73] P. Hariharan, J.A. Pople, Theor. Chim. Acta 28 (1973) 213–222.
[74] A. Vlĉek, S. Zalis, Coord. Chem. Rev. 251 (2007) 258–287.
[75] S.J.A. Van Gisbergen, E.J. Baerends, J.A. McCleverty, T.J. Meyer (Eds.), Comprehensive Coordination Chemistry II, Pergamon, Oxford, 2003, pp. 511–517.
[76] S. Grimme, Rev. Comput. Chem. 20 (2004) 153–218.